IVYSPRING INTERNATIONAL PUBLISHER

Theranostics

2018; 8(16): 4429-4446. doi: 10.7150/thno.26717

Research Paper

Novel multi-drug delivery hydrogel using scar-homing liposomes improves spinal cord injury repair

Qingqing Wang[1,2#], Hongyu Zhang[2#], Helin Xu[2#], Yingzheng Zhao[2], Zhengmao Li[2], Jiawei Li[1], Haoli Wang[1], Deli Zhuge[2], Xin Guo[2], Huazi Xu[1], Salazar Jones[3], Xiaokun Li[2], Xiaofeng Jia[3,4,5]✉, Jian Xiao[1,2]✉

1. Department of Orthopaedics, The Second Affiliated Hospital and Yuying Children's Hospital of Wenzhou Medical University, Wenzhou, Zhejiang,325035 China
2. School of Pharmaceutical Sciences, Wenzhou Medical University, Wenzhou, Zhejiang 325035, China
3. Department of Neurosurgery, University of Maryland School of Medicine, Baltimore, MD, 21201, USA
4. Department of Biomedical Engineering, Anesthesiology and Critical Care Medicine, The Johns Hopkins University School of Medicine, Baltimore, MD 21205, USA
5. Department of Orthopaedics, Anatomy Neurobiology, University of Maryland School of Medicine, Baltimore, MD, 21201, USA

# The first three authors contributed equally to this work

✉ Corresponding authors: Xiaofeng Jia, MD, PhD, Department of Neurosurgery, University of Maryland School of Medicine, Baltimore, MD 21201, USA, Tel: +1-410-706-5026; Email: xjia@som.umaryland.edu; Jian Xiao, PhD, Tel: +86-577-86689989; Email: xfxj2000@126.com

Received: 2018.04.16; Accepted: 2018.07.11; Published: 2018.08.07

Abstract

Proper selection and effective delivery of combination drugs targeting multiple pathophysiological pathways key to spinal cord injury (SCI) hold promise to address the thus far scarce clinical therapeutics for improving recovery after SCI. In this study, we aim to develop a clinically feasible way for targeted delivery of multiple drugs with different physiochemical properties to the SCI site, detail the underlying mechanism of neural recovery, and detect any synergistic effect related to combination therapy.

Methods: Liposomes (LIP) modified with a scar-targeted tetrapeptide (cysteine-alanine-glutamine-lysine, CAQK) were first constructed to simultaneously encapsulate docetaxel (DTX) and brain-derived neurotrophic factor (BDNF) and then were further added into a thermosensitive heparin-modified poloxamer hydrogel (HP) with affinity-bound acidic fibroblast growth factor (aFGF-HP) for local administration into the SCI site (CAQK-LIP-GFs/DTX@HP) in a rat model. *In vivo* fluorescence imaging was used to examine the specificity of CAQK-LIP-GFs/DTX binding to the injured site. Multiple comprehensive evaluations including biotin dextran amine anterograde tracing and magnetic resonance imaging were used to detect any synergistic effects and the underlying mechanisms of CAQK-LIP-GFs/DTX@HP both *in vivo* (rat SCI model) and *in vitro* (primary neuron).

Results: The multiple drugs were effectively delivered to the injured site. The combined application of GFs and DTX supported neuro-regeneration by improving neuronal survival and plasticity, rendering a more permissive extracellular matrix environment with improved regeneration potential. In addition, our combination therapy promoted axonal regeneration via moderation of microtubule function and mitochondrial transport along the regenerating axon.

Conclusion: This novel multifunctional therapeutic strategy with a scar-homing delivery system may offer promising translational prospects for the clinical treatment of SCI.

Key words: spinal cord injury, scar-homing liposome, hybrid hydrogel, neuro-regeneration, combination therapy

Introduction

Spinal cord injury (SCI) remains one of the most devastating conditions in medicine and is pathophysiologically characterized by a series of biochemical cascades that can be injurious beyond the initial injury [1-4]. Although advancing molecular therapies and cellular treatments have been proposed as promising therapies targeting the secondary injury cascade of SCI [5-7], they have not demonstrated satisfactory therapeutic efficacy in the treatment of SCI in clinical trials [8-10]. Possible reasons for these

disappointing outcomes include the following: 1) the lack of regeneration of the damaged axons; 2) the inability of most therapies targeting single pathways to significantly alter the broad, dynamic secondary injury cascades; 3) and subtherapeutic concentrations of pharmacological agents achieved at the injured site, and/or unacceptable systemic side effects [11-13]. Multimodal therapeutic approaches with both neuroprotective and neuroregenerative agents —to counter multiple injury mechanisms—with improved drug delivery should be able to overcome the current barriers to effective SCI therapy.

The limited intrinsic regenerative capabilities of neurons and the inhibitory molecules associated with scars are the two main obstacles to axonal regeneration [14, 15]. However, studies have also demonstrated that overcoming inhibitory signaling alone is of limited benefit [16, 17]. Current methods for boosting the intrinsic growth capacity of axons, such as overexpression of Kruppel-like factor 7 (Klf7) [18] and deletion of the mammalian target of rapamycin (mTOR) regulator phosphatase and tensin homolog (PTEN) [19, 20], are without a clear clinical role as unintended complications, such as epilepsy, cancer, and neuronal hypertrophy, may occur. Fortunately, recent data indicate that low doses of anti-cancer drugs can enhance intrinsic axonal growth and reduce hypertrophic scarring by directly targeting microtubule dynamics [21, 22]. The Food and Drug Administration (FDA)-approved docetaxel (DTX) used here as a microtubule-binding agent may thus represent a novel therapeutic strategy for facilitating axonal regeneration and offer a basis for a multi-targeted therapy. However, this drug elicits little effect in terms of neuroprotection and lesion repair as a monotherapy [23]. Therefore, combinatorial growth factors (GFs), including acidic fibroblast growth factor (aFGF) and brain-derived neurotrophic factor (BDNF), which can target different types of cells in the injured spinal cord, were used here. aFGF plays an essential role in adjusting synaptic plasticity through various cellular mechanisms, as shown in our previous studies [24, 25], and BDNF regulates key processes in neuronal survival and plasticity [26, 27]. These effects are complementary to those of DTX, making GFs promising and excellent candidates for the combined treatment of SCI. However, in view of the disparate pharmacokinetic profiles of the combined drugs (GFs/DTX) having different physiochemical characteristics and non-specific distribution, there are few highly effective strategies for their delivery. Furthermore, there are several obstacles to the use of GFs, including low stabilization, short half-life, and easy degradation.

To overcome these hurdles, in this work, novel scar-homing liposomes modified with tetrapeptides (cystine-alanine-glutamine-lysine (CAQK)) were first constructed to simultaneously encapsulate BDNF in the inner aqueous compartment and DTX in the lipid membrane (CAQK-LIP-BDNF/DTX). The short peptide CAQK can selectively bind to chondroitin sulfate proteoglycans (CSPGs), which are significantly upregulated at the lesion site after SCI [28, 29]. This coupling enables targeted delivery of the drugs to the injured site. However, the poor ability of both drugs to penetrate the blood-spinal cord barrier (BSCB), low drug accumulation and short retention time make their penetration through the deeper injured spinal cord difficult, and the topical use of CAQK-LIP is hampered by their liquid states. Thus, CAQK-LIP-BDNF/DTX was further added into a novel cold heparin-modified poloxamer (HP) solution. Furthermore, aFGF, with a specific high affinity for heparin, was ingeniously embedded in the HP for controlled release. The cold CAQK-LIP-GFs/DTX@HP solution rapidly converted into a three-dimensional hybrid hydrogel (CAQK-LIP-GFs/DTX@HP) *in situ* at the injured spine in response to body temperature after local administration. An extensive study of the physicochemical features and the biocompatibility of the complex was performed to ensure its applicability in SCI. Moreover, *in vivo* and *in vitro* testing were performed with the aim of demonstrating the targeting of the CAQK peptide to the lesion scar after SCI. Multiple comprehensive evaluations, including histological, imaging, and functional assessments, were performed to investigate the profound effect of CAQK-LIP-GFs/DTX@HP both *in vivo* and *in vitro*. Importantly, the detailed mechanisms, including microtubule dynamics and energy transportation, were tested to clarify SCI pathology and pharmacology in greater detail. Overall, this study is significant because it validates a more precise and efficient delivery system for co-loading multiple drugs with distinct physicochemical properties to promote the repair of SCI.

Methods

Preparation of HP matrix with CAQK-liposomes loaded with GFs and DTX (CAQK-LIP-GFs/DTX@HP)

Poloxamer 407 was purchased from Sigma-Aldrich (St. Louis, MO, USA). The synthesis of aFGF-HP according to the 1-ethyl-3-(3-dimethyl-aminopropyl)-carbodiimide (EDC)/N-hydroxysuc-cinimide (NHS) method was previously described [25]. The short peptides (sequences CAQK and

alanine-alanine-alanine-alanine (AAAA)) binding stearic acid with or without 5-carboxyfluorescein (5-FAM) were synthesized by GL Biochem (Shanghai, China). CAQK-LIP-BDNF/DTX was prepared by a reverse evaporation method (**Figure 1**). Briefly, 98 mg phospholipids, 2 mg cholesterol, and 50 μg docetaxel were added to 6 mL dichloromethane. Then, 1 mg BDNF was added to the mixture, and the solution was sonicated for 15 s (100 W, 2 s/3 s = work/stop) to achieve a stable emulsion. The emulsion was rotated and evaporated on a rotary evaporator for complete drying. Then, 4 mL phosphate-buffered saline (PBS) and 200 μL CAQK (0.5 mg/mL) were added, and the solution was sonicated for 20 min to disperse the liposomes (200 W, 2 s/3 s = work/stop). The lyophilized aFGF-HP powder was mixed with the CAQK-LIP-BDNF/DTX solution under modest stirring, and the mixture was stored at 4 °C overnight to form the CAQK-LIP-GFs/DTX@HP solution as previously described. The CAQK-LIP@HP solution was prepared without adding DTX or GFs.

Characterization of HP, CAQK-LIP, CAQK-LIP-GFs/DTX, and CAQK-LIP-GFs/DTX@HP

The particle sizes and size distributions of CAQK-LIP and CAQK-LIP-GFs/DTX were measured using a dynamic light scattering detector (Zetasizer Nano ZS90, Malvern, UK) at 25 °C. The surface morphologies and pore sizes of HP and CAQK-LIP-GFs/DTX@HP were observed with a scanning electron microscope (SEM, Hitachi, Japan). The hydrogels were freeze-dried and sputter-coated with gold followed by scanning analysis. The pore size was determined by imaging 20 random pores followed by analysis with ImageJ software. A rheometer (TA-AR-G2) was used to measure the rheological behaviors of HP and CAQK-LIP-GFs/DTX@HP using stainless steel parallel flat plates (25 mm). The transition temperature was detected at different temperatures ranging from 9.5 to 40.5 °C with 10 rad/s shear frequency and 1% shear strain.

Primary cortical neuron cultures and drug treatment

Primary cortical neurons were extracted from the embryos of pregnant Sprague-Dawley (SD) rats (E18) as previously described [30]. To evaluate the effects of DTX on axonal growth, primary cortical neurons were plated into poly-L-lysine-coated 12-well plates (Sigma Aldrich) with pre-equilibrated medium supplemented with 3.34 μg/mL CSPGs (chicken extracellular chondroitin sulfate proteoglycans, Millipore) dissolved in dimethyl sulfoxide (DMSO) at 1×10^5 cells/well. After two days, the cells were treated with DMSO or varying concentrations of DTX (0.5 nM, 1 nM, 2 nM, 5 nM, 10 nM) for 72 h. To evaluate the effects of hydrogels, neurons were plated in 12-well plates (1×10^5 cells/well) with or without 3.34 μg/mL CSPGs for 48 h, then 20 μL hydrogels (CAQK-LIP-GFs@HP, CAQK-LIP-DTX@HP, CAQK-LIP-GFs/DTX@HP; containing 5 μg/mL aFGF/BDNF and/or 50 μg/mL DTX) were added into the transwell inserts (pore size 0.4 mm) and co-incubated for 72 h. After that (DIV5, 5 days *in vitro*), cells were fixed with paraformaldehyde (4%) and prepared for immunofluorescent staining, which will be described later.

SCI model and drug treatment

Adult female Sprague-Dawley rats (220-230 g, n=152) were provided by the Animal Center of the Chinese Academy of Science (Shanghai, China) and were randomly divided into three groups: sham (n=9), SCI (n=30), CAQK-LIP-GFs@HP (n=24), CAQK-LIP-DTX@HP (n=27), CAQK-LIP-GFs/DTX@HP (n=25), LIP-GFs/DTX@HP (n=24) and CAQK-LIP-GFs/DTX solution group (n=13). All the rats were kept in individually ventilated cages (IVC, 4 rats per cage) in the specific pathogen-free (SPF) room. All the surgical procedures and postoperative care were performed in compliance with the guidelines of the Chinese National Institutes of Health. The surgeries were performed as previously described [31]. In brief, all the animals were anesthetized with 8% (w/v) chloral hydrate (3.5 mL/kg, i.p.) and underwent a laminectomy at the T9-T10 vertebra. After the spinal cord was fully exposed, a contusion injury was inflicted on the spinal cord from a height of 50 mm using a MASCIS Impactor (W.M. Keck Center for Collaborative Neuroscience Rutgers, The State University of New Jersey, USA). Then, 10 μL CAQK-LIP-GFs/DTX solution, CAQK-LIP-GFs@HP, CAQK-LIP-DTX@HP, CAQK-LIP-GFs/DTX@HP, or LIP-GFs/DTX@HP (containing 1 mg/mL aFGF/BDNF and 50 μg/mL DTX) hydrogels were locally delivered using a specialized microsyringe (26 G, an inner diameter of 0.25 mm, an outer diameter of 0.46 mm, 30° bevel, 1 cm long needle, Difa instrument, CO., LTD, Shanghai, China). Postoperatively, carprofen (5 mg/kg s.c.) was used to relieve the pain of the rats, cefazolin sodium (25 mg/kg, i.m.) was used to prevent infections and the bladders were manually emptied three times a day.

Detection of the targeting properties of CAQK peptides *in vivo* and *in vitro*

Three days after SCI, the rats were intravenously injected with 500 μL CAQK-5-carboxyfluorescein

(5-FAM) or AAAA-5-FAM as a control. The animals were perfused with PBS and subsequently with 4% formaldehyde 6 h after injection. The spinal cords were collected and sectioned into 10-μm-thick slices using a cryostat. The fluorescence of the 5-FAM in the spinal tissues was observed with a confocal microscope. Additionally, an *in vivo* spectrum imaging system (IVIS) was used to detect the targeting properties of the CAQK peptides. In brief, the rats were intravenously injected with 500 μL AAAA-LIP- indocyanine green (ICG) and CAQK-LIP-ICG solution 3 days after SCI. The ICG biodistribution analysis was performed at 15 min and 6 h with a 710 nm excitation wavelength and a 785 nm filter to quantify the fluorescence. Primary hippocampal astrocytes were extracted from the SD neonatal rats (P1-2), as a previous study described [32], and were cultured in complete DMEM/F12 medium that was changed every 3-4 days. Astrocytes were seeded into 6-well plates in 1.5 mL medium and cultured at 37 °C under 5% CO_2 for 48 h. After that, hydrogen peroxide solution (H_2O_2, 100 μM) was added into the medium for 6 h to active astrocytes, as described in our previous studies [25, 32], and then the medium was replaced with new medium with AAAA-5-FAM or CAQK-5-FAM solution (1 μg/mL). After 4 h of incubation, the cells were washed thrice and fixed with PBS. Finally, the cells were observed using a confocal laser scanning microscope (TCS SP8, Leica, Germany).

Functional behavior evaluation

Locomotion recovery was assessed using the Basso-Beattie-Bresnahan (BBB) locomotion scale and the footprint test at 0, 3, 7, 14, 21, 28 and 56 d after SCI [33]. Briefly, the BBB locomotion rating scale ranges from 0 to 21 points [34]. Footprint analysis was performed by dipping the animal's hind paws in red dye as described previously [35]. The animal was then allowed to walk across a narrow box (1 m in length and 7 cm in width), its footprints were scanned, and the resulting digitized images were analyzed. The outcome measures were obtained by three independent examiners who were blinded to the experimental conditions.

Histology and immunofluorescence

For *in vitro* Tuj-1, ace-tubulin, tyr-tubulin, and growth cone staining, neurons were placed on coverslips in 12-well plates and treated as described above. After treatment, the cells were fixed in 4% paraformaldehyde and permeabilized in PHEM buffer (60 mM PIPES, 25 mM HEPES, 5 mM EGTA, and 1 mM MgCl), as previously described [24], for immunofluorescence staining. For assessment of *in vivo* immunofluorescence, spinal cords were collected and post-fixed in 4% paraformaldehyde at 4°C overnight, dehydrated in alcohol, and then paraffin embedded. Sagittal sections containing the lesion site were sectioned on a cryostat set at 5 μm thickness. Then, the cells and slices were incubated with 5% BSA for 30 min at 37 °C and then were incubated at 4 °C overnight with the following primary antibodies: glial fibrillary acidic protein (GFAP, 1:500, Santa Cruz), CD 68 (1:1500, Abcam), NeuN (1:1000, Abcam), cleaved-caspase3 (1:200, Cell Signaling Technologies), laminin (1:1000, Abcam), neurofilaments 200 (NF-200,1:10000, Abcam), Tuj-1 (1:1000, Abcam), myelin basic protein (MBP, 1:500, Cell Signaling Technologies), Ace-tubulin (1:1000, Cell Signaling Technologies), Tyr-tubulin (1:1000, Abcam), dynein (1:500, Sigma-Aldrich) and F-actin (1:2000, Abcam). Subsequently, the sections were incubated with AlexaFluor 488 or cy5 donkey anti-rabbit/mouse secondary antibodies for 1 h at 37 °C. Finally, the sections were incubated with DAPI (Solarbio, Beijing, China) for 5 min and washed with PBS. Terminal deoxynucleotidyl transferase (TdT) dUTP nick end labeling (TUNEL) was performed to identify cell apoptosis at 7 d after SCI using In Situ Cell Death Detection Kit (Roche Molecular Biochemicals). For histopathological examination, tissues were stained with hematoxylin-eosin (H&E) following the manufacturer's instructions.

Quantitative image analysis

Quantitative analysis of axonal length *in vitro* was carried out by measuring the longest neurite per neuron for an average of 10 representative neurons per image and 4 representative images using ImageJ software with NeuronJ and image science plugins. The average distance of regeneration *in vivo* per section was defined as the distance between the rostral lesion margins (delineated by GFAP immunostaining). Quantitative measurement of the NF-200, Ace-tubulin and laminin-positive area in the lesion (delineated by GFAP immunostaining) was assessed by pixel counts of positive areas using Adobe Photoshop software [36]. Lesion areas from H&E-stained images (dotted black lines) were measured using ImageJ software. Three sagittal representative sections covering the left, middle and right sides of the spinal cord were measured.

Statistical analysis

The results are presented as mean ± SEM. Differences between groups in BBB scores and body weight throughout time were detected using repeated measurement two-way mixed ANOVA, followed by Tukey test to detect differences between groups.

One-way ANOVA plus Tukey test or Kruskal–Wallis analysis (non-parametric ANOVA) plus Dunn's multiple comparisons (when the data failed the assumptions of one-way ANOVA) were used to test differences between groups at specific times. Two-way ANOVA was conducted to examine the effects of time and different treatments on the level of TNF-α or IL-6. In all the analyses, $p<0.05$ was considered statistically significant.

Results

DTX promoted axon extension at low doses

To detect whether DTX has dose-dependent effects on axon regeneration in a non-permissive condition (in the presence of CSPGs), different concentrations of DTX were administered to neurons and immunofluorescence staining was performed at DIV5. As shown in **Figure S1A-B**, in the presence of CSPGs, the neurites were short, and there was no obvious difference in length between axons and dendrites. However, DTX lengthened axons when applied at the concentration range of 0.5-5 nM and 1 nM DTX produced the longest axons. Meanwhile, the toxicity of DTX was evaluated by Cell Counting Kit-8 (CCK-8) assay. Neurons were treated for 48 h with different dosages of DTX. The results showed that DTX had no cell cytotoxicity on neurons at the concentration of 10 nM (**Figure S1C**). These data indicate that the microtubule-stabilizing agent DTX had a positive effect on axon growth at low doses. Therefore, DTX was used in conjunction with GFs with expected additional therapeutic effects for SCI treatment.

Characterization of the complex hydrogels

CAQK-LIP-GFs/DTX@HP was constructed as displayed in **Figure 1A**. To determine whether this combinatorial hydrogel is suitable for drug delivery in SCI treatment, various characteristics were tested. As illustrated in **Figure 1B**, the particle sizes and polydispersity index (PDI) of the blank LIPs and CAQK-LIP-GFs/DTX were determined to be 159.94 ± 4.92 nm, 0.154 ± 0.02 and 176.29 ± 5.34 nm, 0.149 ± 0.01 respectively, which indicated that drug loading slightly increased the size of the liposomes. The zeta potentials were not significantly different between the empty liposomes (-9.43 ± 0.12 mV) and CAQK-LIP-GFs/DTX (-9.57 ± 0.14 mV), which indicated that the drug had been encapsulated into the liposomes. Three-dimensional and porous sponge-like structures with interconnected inner pores in HP and CAQK-LIP-GFs/DTX@HP were observed by scanning electron microscopy (SEM). The micromorphologies and the pore sizes of these two hydrogels did not markedly differ with (92 ± 12.98 μm) or without the loaded drugs (76.83±9.49 μm). This structure allowed the liposomes to diffuse through the pores and allowed for the release rate to be controlled (**Figure 1C**). Subsequently, the *in vitro* release profiles of aFGF, BDNF, and DTX from CAQK-LIP-GFs/DTX and CAQK-LIP-GFs/DTX@HP were recorded. As illustrated in **Figure 1D-F**, compared with the release from CAQK-LIP-GFs/DTX, the overall releases of BNDF and DTX from the CAQK-LIP-GFs/DTX@HP were comparatively slow, although a small initial burst release corresponding to 21% of the total BDNF and 23% of the total DTX was observed on the first day. Furthermore, due to the included heparin, aFGF from CAQK-LIP-GFs/DTX@HP complex exhibited a more sustained release for at least 21 days with no evident burst effect. We then tested whether the hydrogel is suitable for topical application. Rheology tests were conducted and revealed that all the HP-based hydrogels, regardless of drug loading, displayed similar sol-to-gel transitions at approximately 24 °C (**Figure 1G**), which made the HP-based hydrogels suitable for biomedical applications on the spinal cord. Additionally, the drugs and materials used here induced no obvious toxicity or side effects and exhibited good biocompatibility (**Figure S3**), which indicated that this delivery system is a promising candidate for SCI repair.

CAQK-LIPs targeted drug delivery to the injury sites, and HP hydrogels improved drug retention

To test whether CAQK-LIPs could specifically bind to the lesion site after SCI, multiple targeted binding experiments were performed (**Figure 2A**). Based on *in vivo* IVIS spectrum imaging (**Figure 2B**), even though most of the liposomes accumulated in the liver, relatively high fluorescence was observed at the lesion 6 h after tail vein intravenous injection of CAQK-conjugated LIP-ICG (CAQK-LIP-ICG), while there was little fluorescence at the injury site in the control AAAA-LIP-ICG group. The specific binding of CAQK was also confirmed using fluorescence imaging, as illustrated in **Figure 2C**: CAQK-5-FAM exhibited strong binding to the injured spinal cord region, whereas the binding of the control AAAA-5-FAM was negligible. Low binding of CAQK-5-FAM was observed rostral and caudal to the injury center, which suggested that the CAQK peptide could specifically bind to the molecules secreted at the site of the injury. We additionally measured the targeting properties of CAQK *in vitro* using active astrocytes. As illustrated in **Figure 2D**, substantially more CAQK-5-FAM than AAAA-5-FAM adhered to active astrocytes or the extracellular matrix.

Collectively, these data indicate that CAQK peptide could specifically bind to the injury site. Subsequently, to test whether HP hydrogel could prolong the retention time of CAQK-LIPs within the spinal cord, the *in vivo* spinal cord retention and penetration of the different LIP-ICG complexes after local administration were measured using an *in vivo* IVIS spectrum imaging system. As illustrated in **Figure 2E-F**, the fluorescence intensity in the spinal cord became gradually weaker over time. At 48 h, the fluorescence signals of LIP-ICG group had completely disappeared. In contrast, the fluorescence signals of CAQK-LIP-ICG decayed slowly and lasted 72 h or more with a strong signal in the CAQK-LIP-ICG@HP group. These results confirmed that CAQK could enhance binding to the injury site, and the injectable thermosensitive HP hydrogel could prolong the retention of targeted-CAQK-LIPs within the spinal cord.

CAQK-LIP-GFs/DTX@HP improved pathology and motor function after SCI

Comprehensive pathological and functional evaluations were performed to evaluate neural

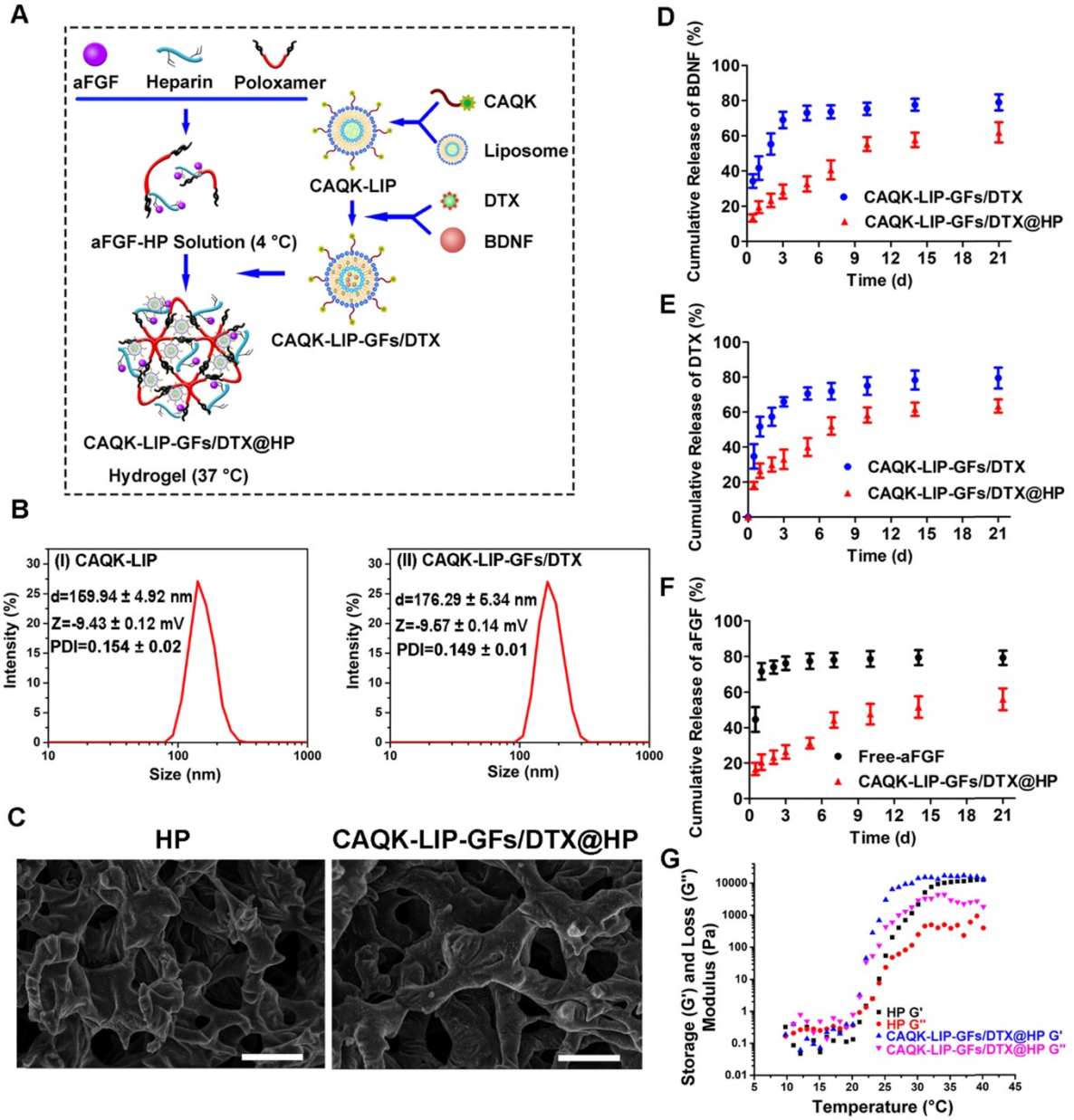

Figure 1. Characterization of the complex hydrogels. (A) Schematic diagram of an injectable hydrogel complex as an *in situ*, targeted multiple drug-delivery system. **(B)** Hydrodynamic particle size distributions of the cysteine-alanine-glutamine-lysine-modified liposomes (CAQK-LIPs) and CAQK-LIPs with docetaxel (DTX) and growth factors (CAQK-LIP-GFs/DTX). **(C)** Scanning electron microscopy images and pore sizes of lyophilized heparin-modified poloxamer hydrogel (HP) and HP hydrogel with affinity-bound acidic fibroblast growth factor (aFGF-HP) combined with a scar-homing delivery system of DTX and brain-derived neurotrophic factor (CAQK-LIP-GFs/DTX@HP). Scale bar = 50 μm. **(D-F)** The release profile of GFs and DTX from the hydrogel. **(G)** Storage (G') and loss (G") moduli of HP and CAQK-LIP-GFs/DTX@HP as a function of temperature from 10 to 40 °C. All experiments were performed in triplicate.

recovery after SCI. Magnetic resonance imaging (MRI) is an effective, noninvasive method for the diagnosis and assessment of SCI and was used to evaluate tissue repair at 28 days after SCI [37]. According to **Figure 3A**, after SCI, the injured site was obviously narrower than the other sites and exhibited a high signal intensity. This pathology was improved by drug treatment. As expected, CAQK-LIP-GFs/DTX@HP treatment markedly enhanced the recovery of the injured spinal cords and promoted a normal morphology, while the CAQK-LIP-GFs@HP and LIP-GFs/DTX@HP treatments also improved the spinal cord morphology to some extent.

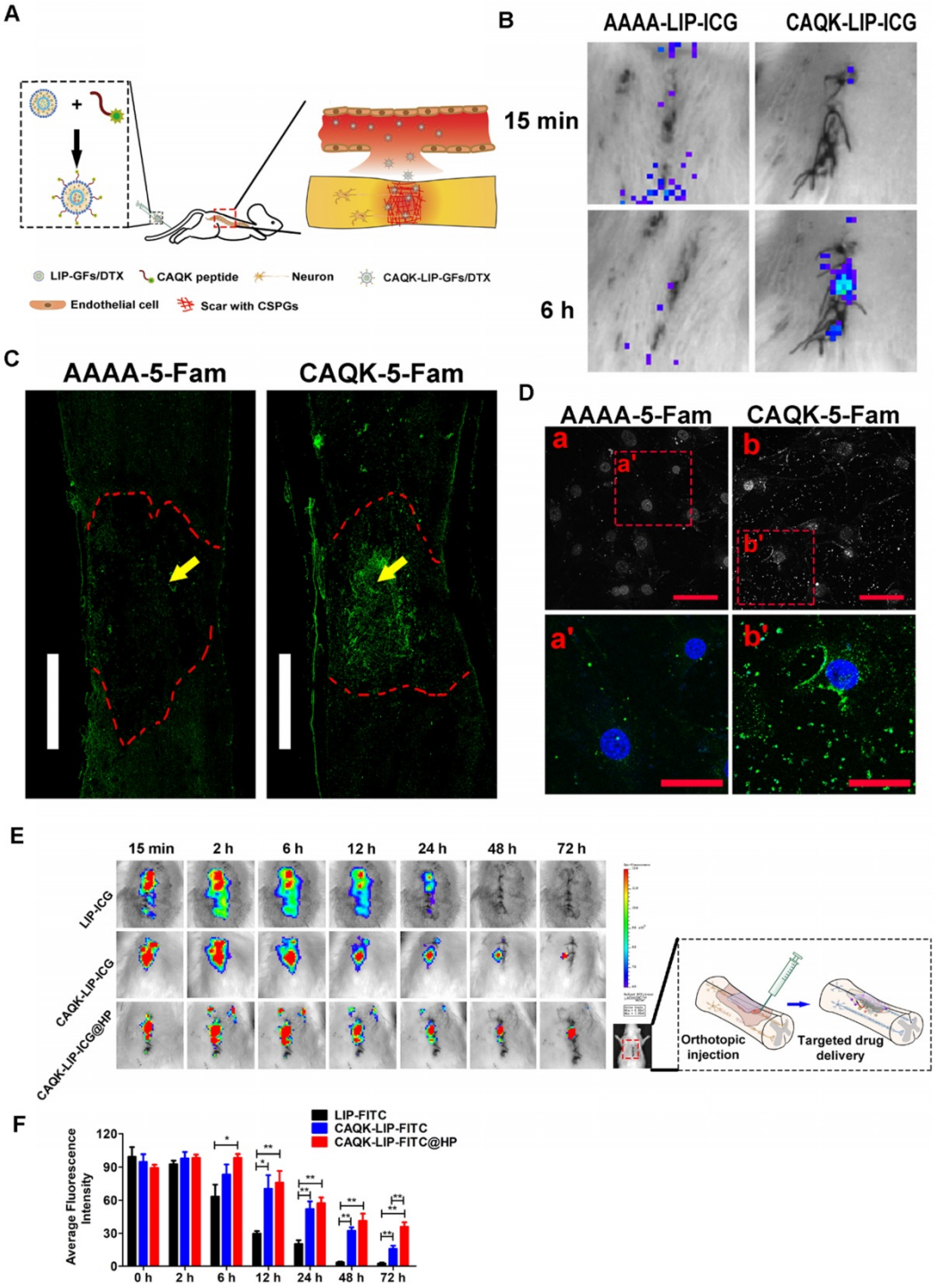

Figure 2. CAQK-LIPs targeted drug delivery to the injury site and HP hydrogels improved drug retention. (A) Schematic diagram of the specific binding of CAQK peptide-modified liposomes to the injury site. **(B)** *In vivo* spectrum imaging system (IVIS) images of the spinal cord injected with indocyanine green (ICG)-labelled peptides at 3 days after spinal cord injury (SCI). **(C)** Fluorescence spinal cord images of rats injected with 5-carboxyfluorescein (5-FAM)-labelled peptides at 3 days after SCI. Scale bar = 1000 μm. **(D)** Fluorescence of the active astrocytes after treating with 5-FAM-labelled peptides for 4 h. **(E)** In vivo spinal cord retention and penetration of the different LIP-ICG complexes measured using IVIS. **(F)** Quantitative analysis of (E). Scale bar = 50 μm. N= 3, *P < 0.05, **P< 0.01.

The changes in the morphology of the injured spinal cord were also observed by H&E staining at 28 d after SCI (**Figure 3B-C**). The spinal cords were severely damaged and exhibited an apparent cavity at the injured site on day 28 after SCI. The treatments with CAQK-LIP-GFs@HP (54.33±3.53% of SCI group) and CAQK-LIP-GFs/DTX@HP (39.33±3.83% of SCI group) induced significant (**p<0.01) protection of the injured spinal cords, as indicated by smaller lesions and less damaged tissue. Functional tests, including the Basso-Beattie-Bresnahan (BBB) locomotion scores (**Figure 3D-F**) and the footprint test (**Figure 3G**), were used to measure whether these imageable pathological effects translated to motor function recovery. Following SCI, the animals exhibited flaccid paralysis with subsequent modest time-dependent recovery. However, the degree of recovery varied between groups. As shown in (**Figure 3D-F**), both the BBB scores of the rats that received CAQK-LIP-GFs@HP (average BBB score of 9) and CAQK-LIP-GFs/DTX@HP (average BBB score of 11) treatment increased relative to the SCI group (average BBB score of 8) 28 days after injury (**p<0.01). On the 56th day after injury, the BBB scores of the CAQK-LIP-GFs/DTX@HP group were significantly higher than those of the CAQK-LIP-GFs@HP and CAQK-LIP-DTX@HP groups (average BBB score of 12, *p<0.05). The footprint test intuitively revealed the restoration of hindlimb movement at 8 weeks post-injury (**Figure 3G**). The rats in the CAQK-LIP-GFs/DTX@HP group were able to crawl, while the rats in the SCI group continued to drag their hind paws. Taken together, these results indicated that, compared to CAQK-LIP-GFs@HP, CAQK-LIP-GFs/DTX@HP treatment had additive therapeutic effects on the motor functions of SCI rats.

CAQK-LIP-GFs/DTX@HP promotes the axonal generation and re-myelination essential for locomotion

We then tested how CAQK-LIP-GFs/DTX@HP induced such promising effects. Axonal regeneration and re-myelination are essential from the perspective of functional restoration of locomotion. Thus, double

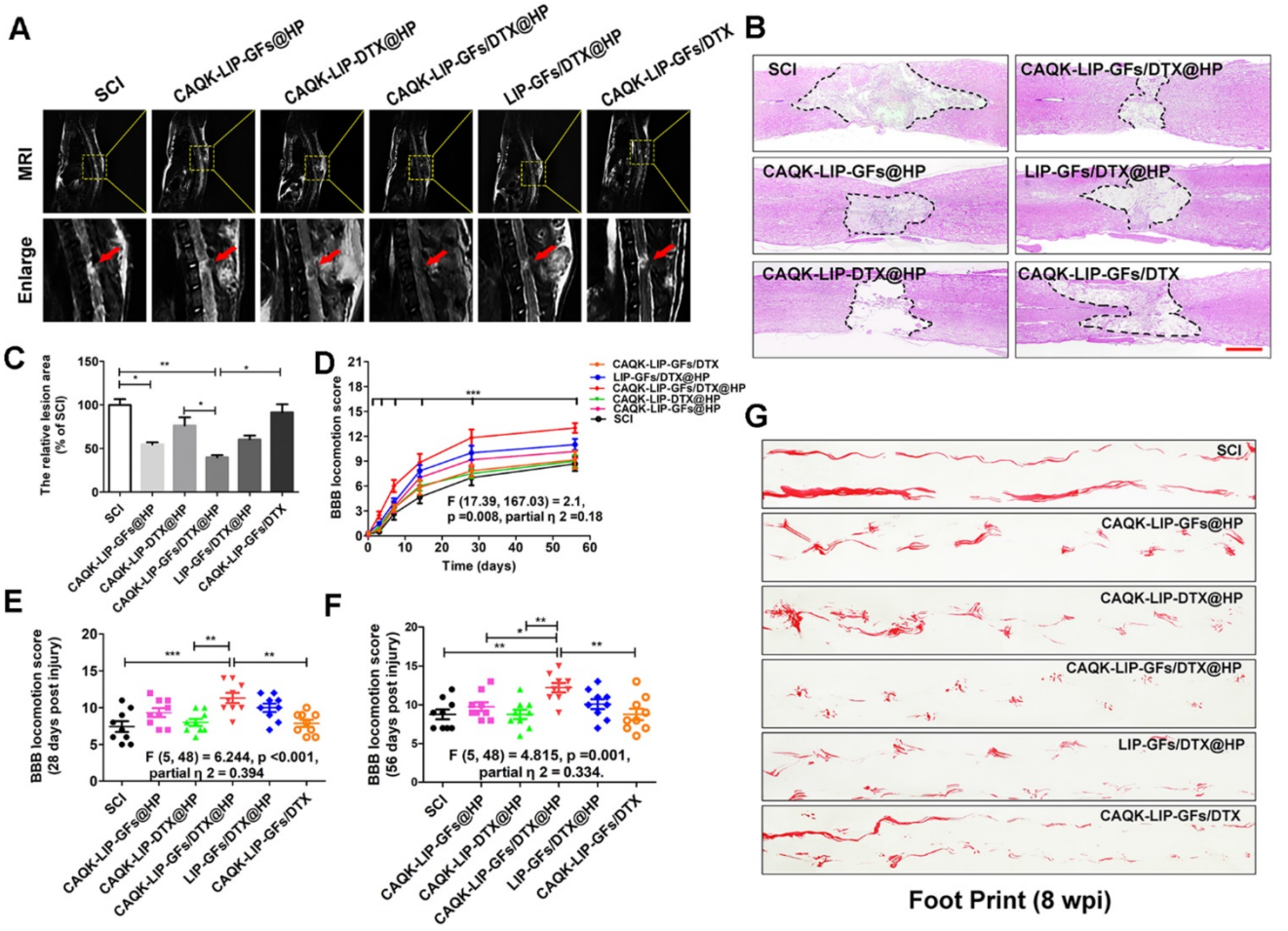

Figure 3. CAQK-LIP-GFs/DTX@HP hydrogels improved pathology and motor function after SCI. (A) MR images of injured spinal cord at 28 days after SCI. **(B)** Representative images from H&E staining at 28 days post-injury. Scale bar = 750 μm. **(C)** Quantification of the lesion area of the spinal cord from H&E staining. **(D-F)** The Basso-Beattie-Bresnahan (BBB) locomotion scores of the different groups. **(G)** Footprint analyses of the different groups. N= 9 per group for BBB score, N= 4 for MRI and H&E staining, *P < 0.05, **P< 0.01.

staining for GFAP (red) and NF-200 (white) was performed to observe the extension of the neurofilaments. In the SCI group, few NF-200-positive axons were observed in the lesion, whereas the CAQK-LIP-GFs@HP and CAQK-LIP-DTX@HP treatment groups presented many NF-200-labeled fibers that passed through the glial scar and presented extended axons. Additionally, the CAQK-LIP-GFs/DTX@HP group had more extended neurofilaments than did the other three treatment groups (**Figure 4A-C**), indicating that the combination of the drugs had better effects, which was also confirmed by biotin dextran amine (BDA) anterograde tracing (**Figure 4D**). Furthermore, compared to control, CAQK-LIP-GFs/DTX@HP promoted the best axonal growth of the embryonic mouse cortical neurons *in vitro* under growth-permissive as well as non-permissive conditions (in the presence of CSPGs), significantly better than CAQK-LIP-DTX@HP and CAQK-LIP-GFs@HP (**Figure 4E-G**). Myelin basic protein (MBP) is essential for myelination during nerve regeneration. As illustrated in **Figure 4H-K**, immunofluorescent staining for MBP in different areas near the epicenter was performed. Although the CAQK-LIP-GFs@HP and LIP-GFs/DTX@HP treatments both increased MBP expression compared to the SCI group, the CAQK-LIP-GFs/DTX@HP treatment increased MBP expression to a greater extent. The western blot analysis results for MBP revealed similar group differences. The TEM results further suggested that the greatest improvements in myelin sheath and axon integrity occurred following treatment with CAQK-LIP-GFs/DTX@HP (**Figure 4L**). In summary, our results demonstrated that both GFs and DTX promoted axonal growth and that the combination of drugs exerted the greatest effects on axonal generation as well as myelin sheath protection.

CAQK-LIP-GFs@HP reduced apoptosis and promoted the rehabilitation of neurons by influencing the inflammatory reaction and macrophage polarization

Next, we aimed to explore how this combined therapy induced axonal regeneration. Neuronal survival is the premise of axon regeneration. To evaluate the role of CAQK-LIP-GFs/DTX@HP in modulating cellular apoptosis after SCI, terminal deoxynucleotidyl transferase (TdT) dUTP nick-end labeling (TUNEL) staining and double immunofluorescence of NeuN and cleaved-caspase3 were performed on neurons at 7 d post-injury (dpi). As illustrated in **Figure 5A-D**, the number of TUNEL-positive cells and the fluorescence intensity of cleaved caspase-3 were markedly increased in the SCI group. CAQK-LIP-GFs@HP and CAQK-LIP-GFs/DTX@HP resulted in remarkable reductions in neuronal apoptosis. By contrast, CAQK-LIP-DTX@HP showed little effect on neuronal protection. To further test the effects of CAQK-LIP-GFs/DTX@HP on the promotion of neuronal plasticity, the expression levels of GAP-43 and nestin, which are two classic indicators of neural regeneration, were tested in each group by western blotting. As illustrated in **Figure 5E-G**, the expression levels of GAP-43 and nestin significantly increased following GF treatment. Among all groups, the CAQK-LIP-GFs/DTX@HP group presented the highest GAP-43 and nestin levels, which revealed that GFs could reduce apoptosis and promote the rehabilitation of neurons and that the delivery system could enhance the effects of the GFs. To detect the mechanism by which the GFs reduced cell apoptosis, inflammatory cells such as macrophages, which invade the lesion site and regulate the "second injury" after SCI, were tested [38]. Macrophages are generally classified into two main categories, i.e., pro-inflammatory macrophages (M1), which provoke secondary damage, and anti-inflammatory (M2) macrophages, which are capable of initiating tissue repair [39]. Examinations of the relative expression levels of pan-macrophage/monocyte ($CD68^+$), M1 ($CD86^+$) and M2 ($CD206^+$) marker proteins by immunofluorescence and western blotting revealed that following SCI, there were several cavities full of $CD68^+$ cells at the injury site (**Figure 5H-K**). CAQK-LIP-GFs@HP treatment markedly reduced inflammation rostral and caudal to the injury, although it did not significantly change the inflammation at the epicenter. The relative level of CD206 protein in the CAQK-LIP-GFs@HP group was approximately 5-fold higher than that of the SCI-only animals at 7 dpi. In contrast, the CD86 protein levels were generally reduced by CAQK-LIP-GFs@HP treatment (**Figure 5L-N**). These results indicated that GFs can reduce apoptosis and promote neuronal growth, possibly impacting the inflammatory reaction and macrophage polarization.

CAQK-LIP-DTX@HP reduces fibrotic scar tissue and CSPGs at the injury site

Trauma to the spinal cord can result in seal-like scar tissue in the lesion zone, which is filled with dense cellular components and a connective extracellular matrix (ECM). The roles of the scar after SCI are complicated and controversial [40-42]. However, a hypertrophic fibrotic scar with excessive expression of chemical inhibitory factors (e.g., CSPGs, myelin-associated glycoproteins (MAG) and Nogo) poses an inhibitory environment for regeneration [43, 44]. As illustrated in **Figure 6A-B, F-G**, after treatment with CAQK-LIP-DTX@HP, the rats exhibited a

significant reduction in laminin- and fibronectin-positive fibrotic scarring at 28 dpi. However, GFAP expression did not markedly differ among the groups, which indicated that the neuroprotective glial sealing of the injury site at the border was not affected by the treatment (**Figure 6C**) [41]. These results were confirmed by western blot analysis (**Figure 6D-E**). CSPGs (including neurocan and NG2), accompanied by reduction of the fibrotic scar, were significantly reduced by CAQK-LIP-DTX@HP treatment (**Figure 6H-J**). Collectively, these data suggest that CAQK-LIP-DTX@HP could significantly reduce inhibitory factors and remodel fibrotic scar tissue.

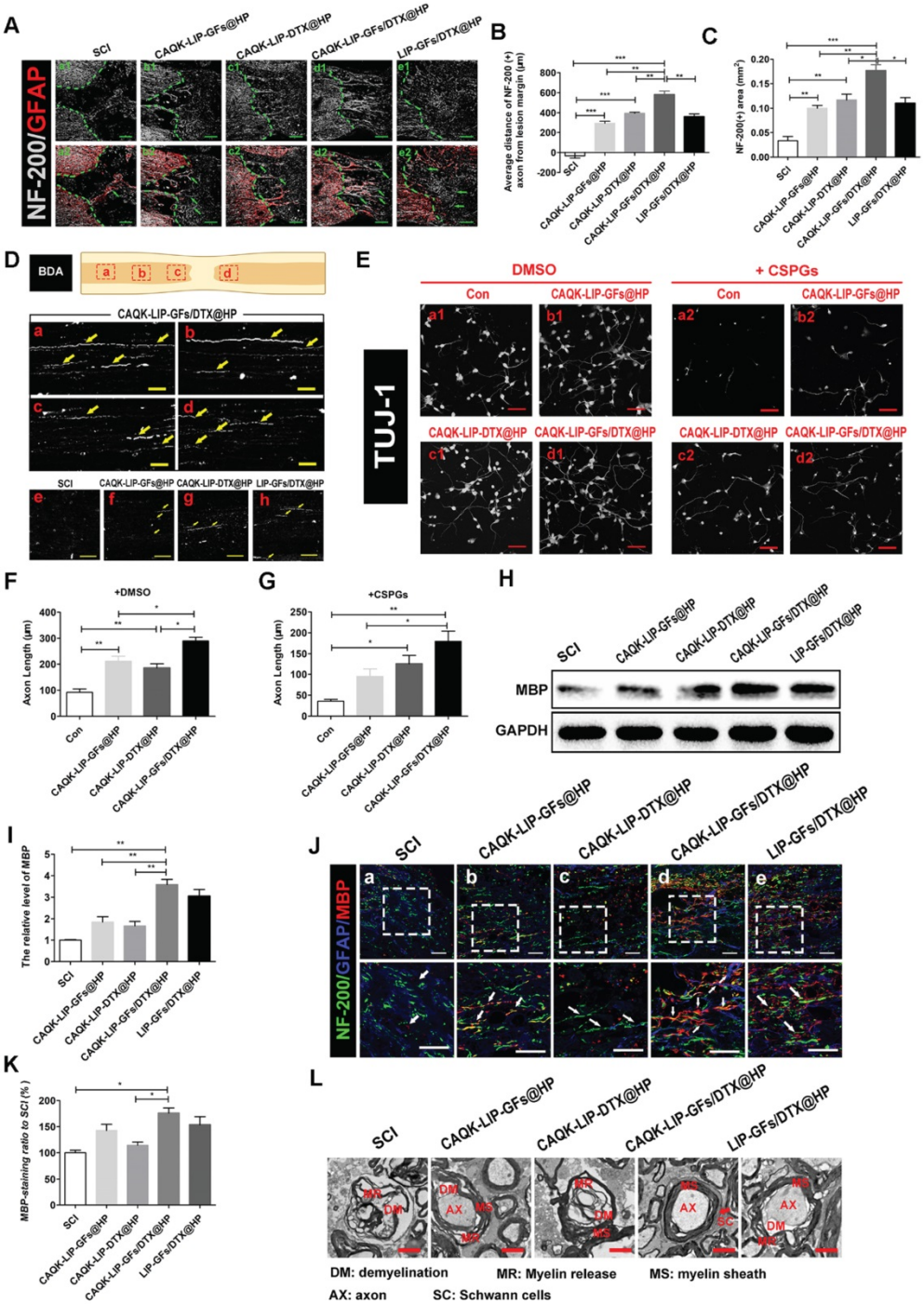

Figure 4. CAQK-LIP-GFs/DTX@HP promotes axonal generation and re-myelination essential for locomotion. (A) Representative images containing astrocytic and neurofilament (NF-200) immunofluorescence on spinal cord sections at 28 days after SCI. Scale bar = 150 μm. **(B-C)** Quantitative analysis of average distance of NF-200 positive axon from lesion margin and NF-200 positive axon area in the lesion. N= 3. **(D)** The expression of biotin dextran amine (BDA) protein in the immunofluorescence staining at different positions of the spinal cord on the 28th day after SCI. Scale bar = 50 μm. **(E)** Beta-3 tubulin (Tuj-1) immunolabeling of neurons with or without inhibitory chondroitin sulfate proteoglycans (CSPGs, 3.34 μg/mL) substrates at DIV5 (days *in vitro for* 5 days). Scale bar = 50 μm. **(F-G)** Neurite length of cortical neurons at DIV5 under indicated conditions. N= 4. **(H-I)** Western Blot (WB) protein expressions and quantification data of MBP in each group. N= 4. **(J-K)** Representative images of NF-200 (green) and myelin basic protein (MBP) immunofluorescence on spinal cord sections at 28 days after SCI. Scale bar = 50 μm. **(L)** Transmission electron microscopy images showing the microstructure of the myelin sheath in each group. *P < 0.05, **P< 0.01, ***P< 0.001.

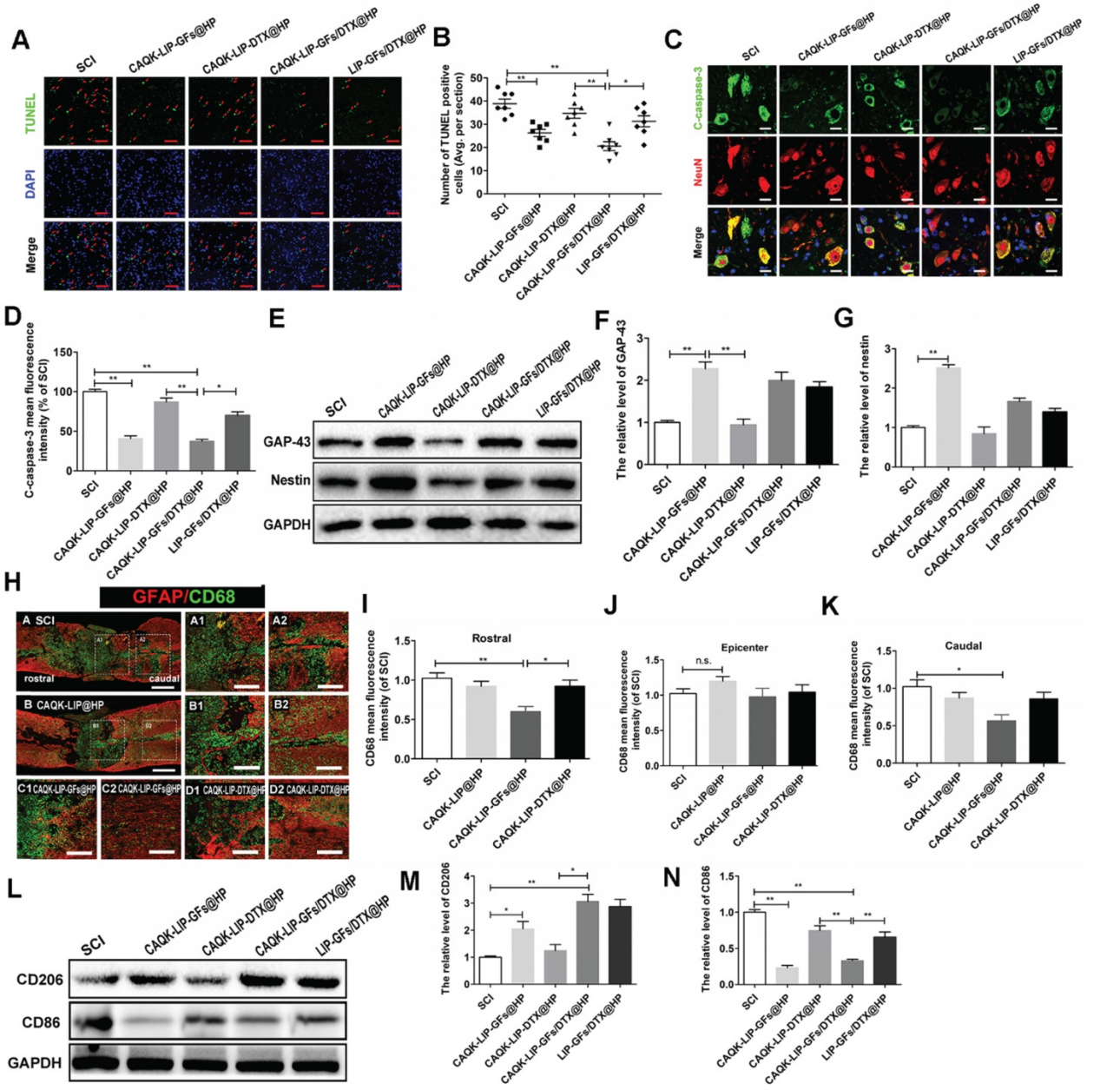

Figure 5. CAQK-LIP-GFs@HP reduced apoptosis and promoted rehabilitation of neurons by impacting the inflammatory reaction and macrophage polarization. (A) Immunofluorescence staining for terminal deoxynucleotidyl transferase (TdT) dUTP nick end labeling (TUNEL, green) of sections from the injured spinal cord in each group. Scale bar = 50 μm. **(B)** Quantitative estimation of apoptotic and TUNEL-positive cells from seven independent sections within 5 mm of the injury epicenter. **(C-D)** Expressions and quantification data of C-caspase-3 from each group. Scale bar = 20 μm. N= 3. **(E-G)** Protein expressions and quantification data of nestin and growth-associated protein 43 (GAP-43) in each group. N= 4. **(H)** Immunofluorescence images of the spinal cord show the relationship of astrogliosis (red) and monocytic phagocytes (CD68, green) in each group. Scale bar = 750 μm (A-B); scale bar = 150 μm (A1-D2). **(I-K)** fluorescence intensity quantification of CD68 in different locations. N= 3. **(L-N)** Protein expressions and quantification data of CD206 and CD86 in each group. N= 3. *P < 0.05, **P< 0.01.

CAQK-LIP-GFs/DTX@HP induced axon extension after SCI by improving microtubule stabilization and moderating the behavior of the growth cone

Numerous studies have suggested that overcoming inhibitory signaling pathways alone results in only slight regeneration [45, 46]; the intrinsic growth ability of injured neurons is more important. To determine the effect of GFs and DTX on microtubule stabilization, which is a novel regulatory mechanism in regenerative growth (**Figure 7A**), acetylated tubulin (Ace-tubulin, a microtubule polymerizing protein) and tyrosinated tubulin (Tyr-tubulin, a microtubule depolymerizing protein) were measured by immunofluorescence staining and western blotting. As illustrated in **Figure 7B-F**, there were few Ace-tubulin-positive axons in the injury epicenter in the SCI group; whereas, CAQK-LIP-GFs@HP and CAQK-LIP-DTX@HP treatment significantly increased the number of Ace-tubulin-labeled fibers that passed through the glial scar. Additionally, the CAQK-LIP-GFs/

DTX@HP treatment group presented more Ace-tubulin-labeled fibers in the injured site than the other three treatment groups, which was mainly due to the combined effects of the drug combination. NF-200 staining yielded similar results: double staining for NF-200 (green) and Ace-tubulin (red) in the axons indicated that microtubule stabilization was essential for axon extension (**Figure 7G**). The roles of the drugs in microtubule stabilization in the neurons *in vitro* were also evaluated. As shown in **Figure 7H-J**, CAQK-LIP-DTX without HP induced axon extension by improving microtubule stabilization *in vitro*; and, CAQK-LIP-GFs/DTX-treated neurons presented significantly longer and polarized single axons than CAQK-LIP-GFs and CAQK-LIP-DTX groups.

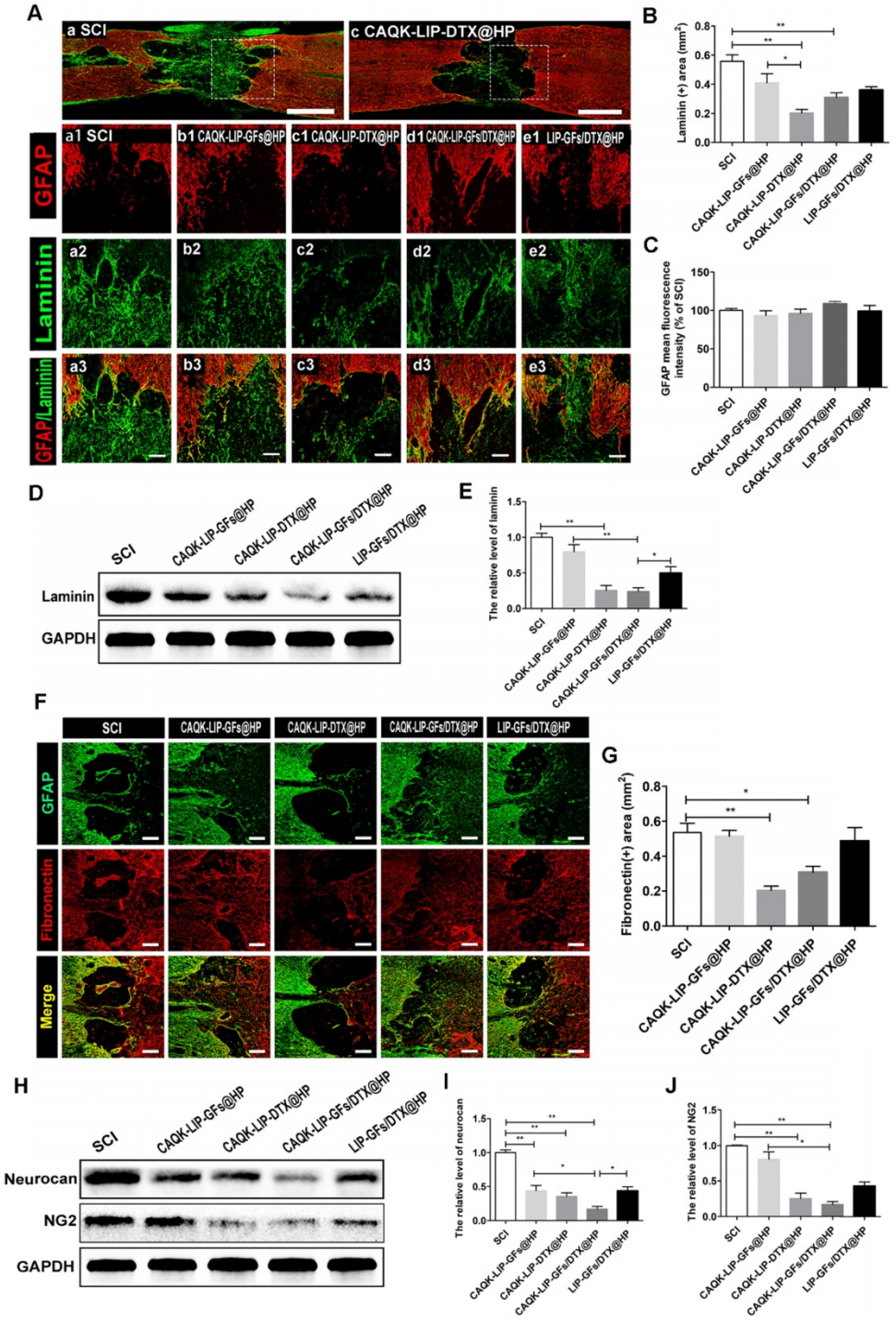

Figure 6. CAQK-LIP-DTX@HP reduced fibrotic scar tissue and CSPGs at the injury site. (A-C) Immunofluorescence staining and quantification data of laminin (green) and GFAP (red) in the spinal cord at 28 days post-injury (dpi). Scale bar = 750 μm (A, C); scale bar = 150 μm (a1-e3). N= 3. **(D-E)** Protein expression and quantification data of laminin in each group. N= 4. **(F-G)** Immunofluorescence staining and quantification data of fibronectin (red) and glial fibrillary acidic protein (GFAP, green) in the spinal cord at 28 days post-injury (dpi). Scale bar = 150 μm. N= 3. **(H-J)** Protein expressions and quantification data of neurocan and neuron-glial antigen 2 (NG2) in each group. N= 4. *P < 0.05, **P< 0.01.

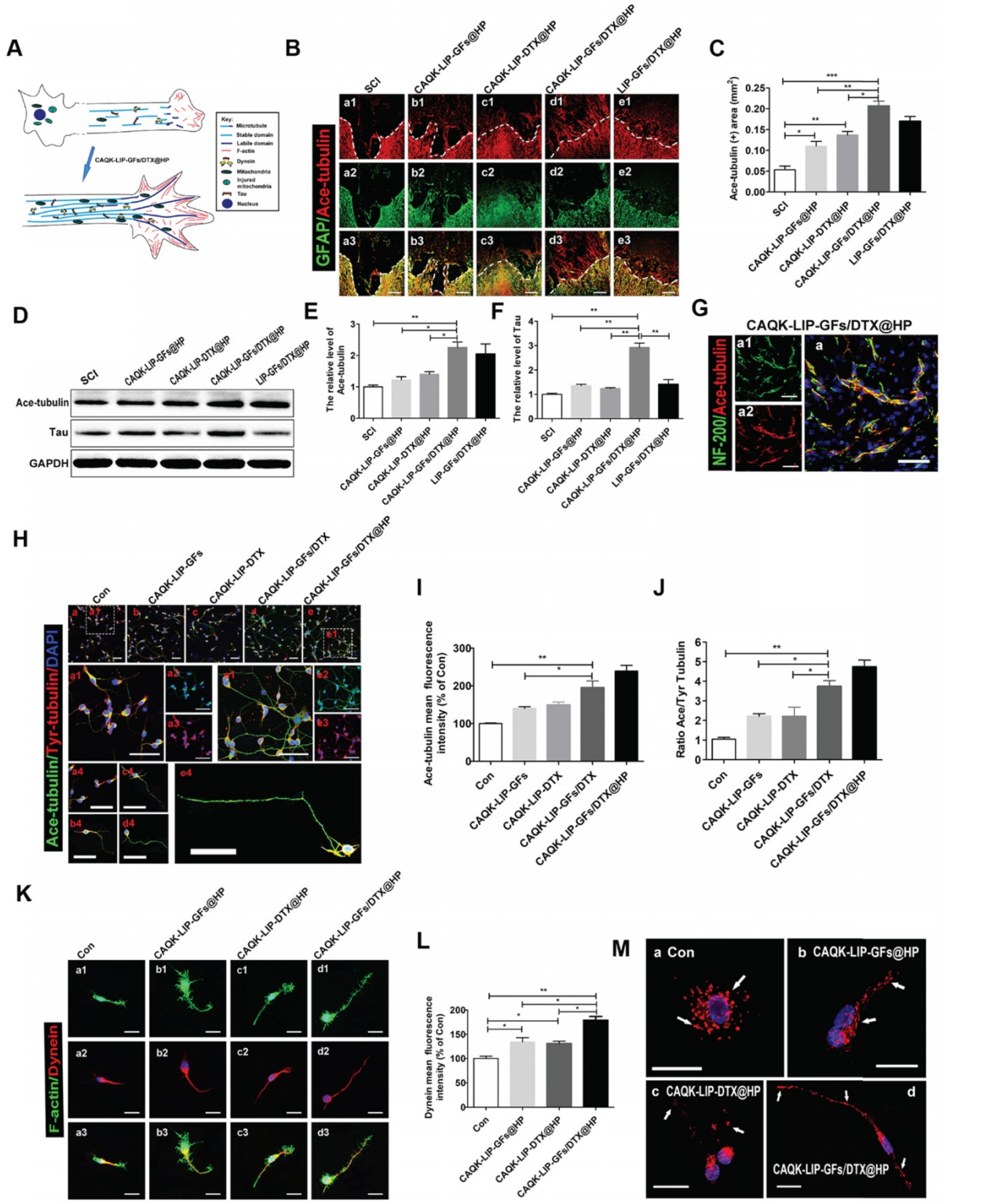

Figure 7. The detailed mechanisms of GFs and DTX in supporting long-range axonal regeneration. (A) Schematic showing how CAQK-LIP-GFs/DTX@HP improves axon regeneration and the relationship between microtubule, dynein and growth cone. **(B)** Co-immunofluorescence images showing GFAP (green) and Ace-tubulin (red) after SCI in each group. Scale bar = 200 μm. **(C)** Quantification data of Ace-tubulin in each group. N= 3. **(D-F)** Representative western blot results of Ace-tubulin and Tau at 14 dpi in each group. N= 4. **(G)** Double staining of NF-200 (green) and Ace-tubulin (red) in axons at the lesion site on the 28th day after SCI. Scale bar = 50 μm. **(H)** Co-immunofluorescence images show Ace-tubulin (green) and Tyr-tubulin (red) in primary cortical neurons at DIV5 (5 days *in vitro*). Scale bar = 50 μm. **(I-J)** Quantification of Ace-tubulin and A/T ratio from (H). N= 4. **(K)** Co-immunofluorescence images showing the distribution of F-actin (green) and dynein (red) in the growth cone at DIV3. Scale bar = 10 μm. **(L)** Quantitative analysis of dynein staining intensity. N= 4. **(M)** Mitochondrial staining images using MitoDsRed (red) at DIV5. Scale bar = 20 μm. *P < 0.05, **P< 0.01, ***P< 0.001.

Meanwhile, the expression of Ace-tubulin and the ratio of Ace to Tyr-tubulin (A/T ratio) were markedly improved, which are associated with axonal extension (**Figure 7H-J**). Furthermore, these effects

were increased by incorporating HP hydrogel. Additionally, Tau protein, which can modulate microtubule dynamics and stabilization, was significantly increased with CAQK-LIP-GFs/DTX@HP treatment (**Figure 7D-F**). The growth cone is not only needed in the initiation of axon regeneration but also required in axonal polarized extension and regrowth [47]. As illustrated in **Figure 7K-L**, compared with the control group, the CAQK-LIP-GFs/DTX@HP, CAQK-LIP-GFs@HP and CAQK-LIP-DTX@HP groups exhibited more robust growth cones with higher intensities of F-actin. Collectively, these findings indicate that both GFs and DTX induced significant microtubule stabilization, pulled the microtubule cytoskeleton toward the leading edges of the neurons, elongated the microtubules and thus promoted axonal growth and migration.

GFs and DTX supported long-range axonal regeneration through different mechanisms

Regenerating axons often need to grow over long distances to rebuild functional circuits. Sustained axonal growth is critically dependent on the regulation of axonal energy transport [48]. Mitochondria, which are essential for dynein to generate ATP-dependent forces on the microtubules, were detected by staining with MitoTracker Red (**Figure 7M**). Following neuronal injury, axonal mitochondria traffic was increased, and most of the mitochondria were clustered around the cell nuclei. The mitochondria were gradually transported to the axon after treatment with CAQK-LIP-DTX@HP. Interestingly, the mitochondria were efficiently elongated after administration of CAQK-LIP-GFs@HP. Furthermore, extensive connected and tubular mitochondria were induced by CAQK-LIP-GFs/DTX@HP and were lined along the axon. Collectively, CAQK-LIP-GFs/DTX@HP may have effects on promoting mitochondrial fusion and regulating mitochondrial localization in neuronal axons, which were conducive to long-range axonal regeneration.

Discussion

In a previous study, we described a thermosetting hydrogel with affinity-bound aFGF for local administration into the SCI site [25]. The study showed that aFGF-HP exerted neuroprotective effects and created advantageous conditions for BSCB and functional restoration. However, existing research has confirmed that strategies that only target one inhibitory substance or only aim to promote axonal regeneration have limited efficacy for the recovery of SCI, which has a multifaceted nature [49]. Thus, a combinatorial approach is urgently needed. Various combinatorial approaches involving drugs and interventions including Chondroitinase ABC (ChABC)/neurotrophic factors [50], cells/neurotrophic factors [51, 52], and anti-myelin-associated glycoproteins (MAG)/other anti-inhibitory factors [51, 53, 54], have been proposed for effective regeneration after SCI. Nevertheless, most of them are neuroprotective and do not promote the restoration of severed axonal connections, or they try to overcome only one of the obstacles to regeneration. Most approaches have thus failed in clinical translation for the following reasons: 1) limited regeneration of damaged axons, 2) low delivery efficiency of combinatorial drugs, and 3) low drug concentrations achieved at the target lesion or unacceptable side effects. In this study, we developed a new strategy involving short peptide (CAQK)-modified liposomes simultaneously loaded with water-soluble BDNF and liposoluble DTX that home to the injury site and specifically link with CSPGs after SCI. These targeted liposomes were embedded into a three-dimensional, thermosensitive injectable poloxamer gel matrix, which was also linked with heparin and heparin-binding aFGF (CAQK-LIP-GFs/DTX@HP). The release of DTX from our combinatorial delivery system was demonstrated to be extended to 10 days with the majority of DTX released between days 1 and 5 by different delivery strategies. By encapsulating soluble BDNF within the liposomes in the LIP@HP hydrogel matrix and chemically binding aFGF with heparin in the HP hydrogel, we observed prolonged bioactive release of BDNF over 10 days and release of aFGF over 21 days. In a recent publication, Mann et al. reported a short peptide (sequence CAQK) that can selectively bind to the proteoglycan complexes in injured mouse and human brain [29]. Coupling to CAQK increased injury site accumulation of systemically administered molecules ranging from a drug-sized molecule to nanoparticles. However, it remained to be tested whether CAQK also homes to spinal cord injury. Herein, our *in vivo* IVIS spectrum imaging and immunofluorescence data confirmed that CAQK-conjugated liposomes could specifically bind to the injured site after SCI, in contrast to the control AAAA-peptide. Furthermore, when coated with the HP hydrogel, CAQK-LIP-GFs/DTX@HP was retained for a long time in the damaged area after local administration and homing to the injured spinal cord, providing sustained drug delivery for neuroprotection and neuroregeneration in SCI rats *in vivo*. This targeting approach has the potential for converting agents with unfavorable pharmacokinetic profiles into efficient drugs. Furthermore, the approach could be translated to the clinic because the

CAQK peptide recognizes target molecules in the human injured brain. These promising findings present an effective targeting strategy for the delivery of therapeutics in the clinical management of SCI.

Although the roles of the scar after SCI are complicated and controversial, the hypertrophic fibrotic scar formed at the lesion site after SCI with excessive expression of chemical inhibitory factors poses an inhibitory environment for regeneration [28, 41, 55]. Our data revealed a comparable decrease of fibrotic scarring associated with a decrease of CSPGs, including neurocan and NG2, when CAQK-LIP-DTX@HP was locally delivered to the injury site. However, the neuroprotective glial sealing was not affected as the astrogliosis was similar between CAQK-LIP-DTX@HP-treated injuries and the control group injuries, which indicated that DTX may reduce scarring in a lesion-dependent manner. Furthermore, the cystic cavities that develop following spinal cord injury in rats and humans and are devoid of ECM or axons were expanded in CAQK-LIP-DTX@HP-treated specimens and narrowed when combined with GF administration using CAQK-LIP-GFs/DTX@HP. Interestingly, the cystic cavities were bridged by a low-density ECM in the CAQK-LIP-GFs@HP group, which suggests that GFs might regulate both the synthesis and disassembly of the ECM and induce beneficial ECM remodeling to stimulate tissue repair as well as provide a scaffold for axonal sprouting. These effects might be due to the local immune-modulatory action of GFs and will be discussed below. Various drugs, including anti-CSPGs and Nogo-A inhibitors such as ChABC, IN-1, and 7B12, have been used to reduce scarring and inhibitory molecules [36, 56, 57]. However, only limited sprouting and neurogenesis occur rather than long-distance axonal regeneration, although various inhibitors provide a more permissive environment [58, 59]. This result may be because the inhibitors have a minimal ability to improve the endogenous regenerative capacity of injured neurons.

Encouragingly, we confirmed that CAQK-LIP-DTX@HP significantly facilitated axonal regeneration and promoted axonal extension, thus restoring axonal growth despite the presence of inhibitory molecules such as CSPGs. Our in-depth evaluation of the mechanism of action of DTX in axonal regeneration demonstrated that DTX regulated the dynamic rearrangement and stabilization of microtubules, which are essential for axonal outgrowth [60, 61], by improving the expression of Ace-tubulin and increasing the A/T ratio. DTX also strengthened and improved the motility of the growth cone, as revealed by the increasing intensity of F-actin staining, and thus elongated the microtubules by regulating the forces imposed on the microtubules by molecular motor proteins [47, 62, 63]. DTX further disentangled the coupled interaction of microtubules and F-actin, which facilitated further polymerization and stabilization of the overall cytoskeleton structure in the growth cone and filopodial extensions. Moreover, we suggested that GFs positively synergize with DTX in promoting neurite outgrowth and axonal regeneration probably by upregulating the receptors of trophic factors such as Trks, mediating microtubule stabilization, and decreasing the sensitivity of growth cones to extrinsic inhibitory molecules, as has been reported [64-66]. Furthermore, a tremendous amount of energy is needed to support the long-range axonal transport of materials [67]. As such, the regulation of axonal mitochondria transport is critical for sustaining regenerative growth [68]. Interestingly, we found that DTX was conducive to the transport of mitochondria to the ends of the axons and that GFs might induce mitochondrial fusion and promote the sustained transport of mitochondria to the axons, which may partially explain why the combination of drugs exerted the greatest effects on axonal generation.

Another major factor in the efficacy of CAQK-LIP-GFs/DTX@HP in treating SCI is the neuroprotection of GFs, including their local immune-modulatory action and effects in promoting neuronal plasticity [46]. It is widely acknowledged that a pronounced microglia/macrophage response is induced after SCI via the release of pro-inflammatory cytokines, nitric oxide (NO), and reactive oxygen species (ROS) by M1 macrophages [69, 70], which leads to ECM degradation, scar formation, neuron death and axon retraction [71, 72]. Our data suggest that GFs likely promote tissue repair and ECM remodeling in part by inhibiting the spread of M1 macrophages and increasing the activation and/or proliferation of M2 macrophages during the early post-lesion phase. Furthermore, the modified inflammatory reaction also helps to enhance cell survival, prevent axon retraction and improve the growth potential and plasticity of neurons. Functional recovery is essential for a new strategy in SCI repair. From the functional results (**Figure 3**), we can see that the BBB scores of both CAQK-LIP-GFs@HP and CAQK-LIP-GFs/DTX@HP groups increased relative to the SCI group 28 days after injury; but, the latter had a better effect. On the 56th day after injury, the BBB scores of the CAQK-LIP-GFs/DTX@HP group were significantly higher than those of the CAQK-LIP-GFs@HP and CAQK-LIP-DTX@HP groups. These results indicated that although DTX itself does not significantly improve motor function in SCIrats, it can increase the effect of GFs, especially for

long-term locomotion recovery. This positive effect may be due to the combined effects of GFs and DTX in targeting multiple aspects of SCI, as described above.

Compared with other published works, our present study not only combines both neuroprotective and neuroregenerative agents to target the multiple aspects of SCI, but also provides a new strategy for targeted co-delivery of macromolecular water-soluble proteins and small molecule liposoluble compounds. However, the underlying mechanisms of DTX on promoting axon growth and the relationships between axon growth, scar reduction, and functional recovery remain to be further elucidated in future research. Prior to clinical translation of this hybrid hydrogel, additional research is needed on the interaction of multiple drugs within the hydrogel and their *in vivo* biodegradation. Furthermore, systemic administration of the scar-targeted CAQK-LIP-GFs/DTX can be considered a potential strategy for chronic SCI intervention in the future using modified liposomes that can cross the BSCB and are not ingested by the liver.

Conclusion

The present study reported a novel multi-drug delivery hydrogel system using scar-homing liposomes for SCI repair. The DTX we used here was proved to be a novel therapeutic agent for facilitating axon regeneration and offers a basis for multi-targeted therapy by increasing the intrinsic growth potential, initiating the myelination of injured neuron axons and reducing inhibitory molecules through directly targeting microtubule dynamics. Moreover, BDNF and aFGF exhibited complementary advantages for SCI repair that included inhibiting the spread of inflammation, promoting neuronal plasticity, and promoting ECM remodeling. A novel scar-homing CAQK-LIP coated with HP hydrogel was first constructed here. This delivery system not only offers a new strategy to simultaneously encapsulate multiple drugs (DTX and GFs) that have different physiochemical characteristics and non-specific distributions but can also deliver these drugs to the injury site in a targeted manner with high efficiency. The system prolongs the half-lives of the drugs and maximizes functional recovery via multiple effects on neural protection and regeneration. Furthermore, the detailed mechanisms, including microtubule dynamics and energy transportation, were studied for the first time for a deeper understanding of the beneficial effects of CAQK-LIP-DTX/GFs@HP. With good biocompatibility, cytocompatibility, and thermosensitivity, this novel targeted multi-drug delivery system offers a promising translational perspective for the treatment of SCI.

Abbreviations

AAAA: alanine-alanine-alanine-alanine; aFGF: acidic fibroblast growth factor; BBB: Basso-Beattie-Bresnahan; BCA: bicinchoninic acid; BDA: biotin dextran amine; BDNF: brain-derived neurotrophic factor; BSCB: blood-spinal cord barrier; CAQK: cysteine-alanine-glutamine-lysine; CCK-8: Cell Counting Kit-8; ChABC: Chondroitinase ABC; CSPGs: chondroitin sulfate proteoglycans; DIV: days *in vitro*; DMEM/F-12: Dulbecco's Modified Eagle Medium/Nutrient Mixture F-12; DMSO: dimethyl sulfoxide; DTX: docetaxel; ECM: extracellular matrix; EDC: 1-ethyl-3-(3-dimethylaminopropyl)-carbodi-imide; EDTA: ethylenediaminetetraacetic acid; ELISA: enzyme-linked immunosorbent assay; FAM: 5-Carboxyfluorescein; FDA: Food and Drug Administration; FM: Fibroblast Medium; FTIR: Fourier transform infrared spectroscopy; GAP-43: Growth associated protein 43; GFAP: Glial fibrillary acidic protein; GFs: growth factors; HBVAFs: Human Brain Vascular Adventitial Fibroblasts; HP: heparin-modified poloxamer; HPLC: high-perfor-mance liquid chromatography; ICG: indocyanine green; Klf7: Kruppel-like factor 7; LIP: liposome; MATP: monoamine-terminated poloxamer; MBP: Myelin Basic Protein; MES: 4-morpholine ethane sulfonic acid; MRI: Magnetic Resonance Imaging; mTOR: mammalian target of rapamycin; NF-200: Neurofilaments 200; NG2: Neuron-glial antigen 2; NHS: N-hydroxysuccinimide; NO: nitric oxide; PBS: phosphate-buffered saline; PDI: polydispersity index; PTEN: phosphatase and tensin homolog; PMSF: phenylmethanesulfonylfluoride; SCI: spinal cord injury; SDS: sodium dodecyl sulfate; SEM: scanning electron microscopy; SPF: specific pathogen free; TUNEL: Terminal deoxynucleotidyl transferase (TdT) dUTP nick end labeling; 5- IVIS: *in vivo* spectrum imaging system.

Supplementary Material

Supplementary methods and figures.
http://www.thno.org/v08p4429s1.pdf

Acknowledgments

This work was supported by the Natural Science Foundation of Zhejiang Province (R18H50001 to J.X.), National Natural Science Foundation of China (81772450 to H.Y.Z., 81722028 and 81572237 to J.X.), Zhejiang Provincial Project of Key Scientific Group (2016C33107 to H.Y.Z.). X. J. was supported partially by R01HL118084 from NIH (to X.J.) and Maryland Stem Cell Research Fund, USA (2018-MSCRFD-4271) (to X.J.).

Competing Interests

The authors have declared that no competing interest exists.

References

1. Andresen SR, Biering-Sorensen F, Hagen EM, Nielsen JF, Bach FW, Finnerup NB. Pain, spasticity and quality of life in individuals with traumatic spinal cord injury in Denmark. Spinal Cord. 2016; 54: 973-9.
2. Rivers CS, Fallah N, Noonan VK, Whitehurst DG, Schwartz CE, Finkelstein JA, et al. Health Conditions: Effect on Function, Health-Related Quality of Life, and Life Satisfaction After Traumatic Spinal Cord Injury. A Prospective Observational Registry Cohort Study. Arch Phys Med Rehabil. 2018; 99: 443-51.
3. Hiremath SV, Hogaboom NS, Roscher MR, Worobey LA, Oyster ML, Boninger ML. Longitudinal Prediction of Quality-of-Life Scores and Locomotion in Individuals With Traumatic Spinal Cord Injury. Arch Phys Med Rehabil. 2017; 98: 2385-92.
4. Ahuja CS, Martin AR, Fehlings M. Recent advances in managing a spinal cord injury secondary to trauma. F1000Res. 2016; 5: 1017.
5. Kwon BK, Tetzlaff W, Grauer JN, Beiner J, Vaccaro AR. Pathophysiology and pharmacologic treatment of acute spinal cord injury. Spine J. 2004; 4: 451-64.
6. Tykocki T, Poniatowski L, Czyz M, Koziara M, Wynne-Jones G. Intraspinal Pressure Monitoring and Extensive Duroplasty in the Acute Phase of Traumatic Spinal Cord Injury: A Systematic Review. World Neurosurg. 2017; 105: 145-52.
7. Nowrouzi B, Assan-Lebbe A, Sharma B, Casole J, Nowrouzi-Kia B. Spinal cord injury: a review of the most-cited publications. Eur Spine J. 2017; 26: 28-39.
8. Widerstrom-Noga E. Neuropathic Pain and Spinal Cord Injury: Phenotypes and Pharmacological Management. Drugs. 2017; 77: 967-84.
9. Nardone R, Florea C, Holler Y, Brigo F, Versace V, Lochner P, et al. Rodent, large animal and non-human primate models of spinal cord injury. Zoology (Jena). 2017; 123: 101-14.
10. Tse CM, Chisholm AE, Lam T, Eng JJ, Team SR. A systematic review of the effectiveness of task-specific rehabilitation interventions for improving independent sitting and standing function in spinal cord injury. J Spinal Cord Med. 2017; 41: 254-66..
11. Muresanu DF, Sharma A, Lafuente JV, Patnaik R, Tian ZR, Nyberg F, et al. Nanowired Delivery of Growth Hormone Attenuates Pathophysiology of Spinal Cord Injury and Enhances Insulin-Like Growth Factor-1 Concentration in the Plasma and the Spinal Cord. Mol Neurobiol. 2015; 52: 837-45.
12. Wilcox JT, Satkunendrarajah K, Nasirzadeh Y, Laliberte AM, Lip A, Cadotte DW, et al. Generating level-dependent models of cervical and thoracic spinal cord injury: Exploring the interplay of neuroanatomy, physiology, and function. Neurobiol Dis. 2017; 105: 194-212.
13. Mironets E, Wu D, Tom VJ. Manipulating extrinsic and intrinsic obstacles to axonal regeneration after spinal cord injury. Neural Regen Res. 2016; 11: 224-5.
14. Liu K, Lu Y, Lee JK, Samara R, Willenberg R, Sears-Kraxberger I, et al. PTEN deletion enhances the regenerative ability of adult corticospinal neurons. Nature neuroscience. 2010; 13: 1075.
15. Dyck SM, Karimi-Abdolrezaee S. Chondroitin sulfate proteoglycans: Key modulators in the developing and pathologic central nervous system. Exp Neurol. 2015; 269: 169-87.
16. Fischer D, He Z, Benowitz LI. Counteracting the Nogo receptor enhances optic nerve regeneration if retinal ganglion cells are in an active growth state. Journal of Neuroscience. 2004; 24: 1646-51.
17. Sengottuvel V, Fischer D. Facilitating axon regeneration in the injured CNS by microtubules stabilization. Communicative & integrative biology. 2011; 4: 391-3.
18. Blackmore MG, Wang Z, Lerch JK, Motti D, Zhang YP, Shields CB, et al. Kruppel-like Factor 7 engineered for transcriptional activation promotes axon regeneration in the adult corticospinal tract. Proc Natl Acad Sci U S A. 2012; 109: 7517-22.
19. Huang Z, Hu Z, Xie P, Liu Q. Tyrosine-mutated AAV2-mediated shRNA silencing of PTEN promotes axon regeneration of adult optic nerve. PLoS One. 2017; 12: e0174096.
20. Park KK, Liu K, Hu Y, Kanter JL, He Z. PTEN/mTOR and axon regeneration. Exp Neurol. 2010; 223: 45-50.
21. Brizuela M, Blizzard CA, Chuckowree JA, Dawkins E, Gasperini RJ, Young KM, et al. The microtubule-stabilizing drug Epothilone D increases axonal sprouting following transection injury in vitro. Mol Cell Neurosci. 2015; 66: 129-40.
22. Sengottuvel V, Fischer D. Facilitating axon regeneration in the injured CNS by microtubules stabilization. Commun Integr Biol. 2011; 4: 391-3.
23. Popovich PG, Tovar CA, Lemeshow S, Yin Q, Jakeman LB. Independent evaluation of the anatomical and behavioral effects of Taxol in rat models of spinal cord injury. Exp Neurol. 2014; 261: 97-108.
24. Li J, Wang Q, Cai H, He Z, Wang H, Chen J, et al. FGF1 improves functional recovery through inducing PRDX1 to regulate autophagy and anti-ROS after spinal cord injury. J Cell Mol Med. 2018; 22: 2727-38.
25. Wang Q, He Y, Zhao Y, Xie H, Lin Q, He Z, et al. A Thermosensitive Heparin-Poloxamer Hydrogel Bridges aFGF to Treat Spinal Cord Injury. ACS Appl Mater Interfaces. 2017; 9: 6725-45.
26. Han S, Wang B, Jin W, Xiao Z, Li X, Ding W, et al. The linear-ordered collagen scaffold-BDNF complex significantly promotes functional recovery after completely transected spinal cord injury in canine. Biomaterials. 2015; 41: 89-96.
27. Tashiro S, Shinozaki M, Mukaino M, Renault-Mihara F, Toyama Y, Liu M, et al. BDNF induced by treadmill training contributes to the suppression of spasticity and allodynia after spinal cord injury via upregulation of KCC2. Neurorehabilitation and neural repair. 2015; 29: 677-89.
28. Haggerty AE, Marlow MM, Oudega M. Extracellular matrix components as therapeutics for spinal cord injury. Neurosci Lett. 2017; 652: 50-5.
29. Mann AP, Scodeller P, Hussain S, Joo J, Kwon E, Braun GB, et al. A peptide for targeted, systemic delivery of imaging and therapeutic compounds into acute brain injuries. Nat Commun. 2016; 7: 11980.
30. Xu K, Wu F, Xu K, Li Z, Wei X, Lu Q, et al. NaHS restores mitochondrial function and inhibits autophagy by activating the PI3K/Akt/mTOR signalling pathway to improve functional recovery after traumatic brain injury. Chemico-biological interactions. 2018; 286: 96-105.
31. Zhou KL, Zhou YF, Wu K, Tian NF, Wu YS, Wang YL, et al. Stimulation of autophagy promotes functional recovery in diabetic rats with spinal cord injury. Sci Rep. 2015; 5: 17130.
32. Ye L, Yang Y, Zhang X, Cai P, Li R, Chen D, et al. The Role of bFGF in the Excessive Activation of Astrocytes Is Related to the Inhibition of TLR4/NFkappaB Signals. Int J Mol Sci. 2015; 17: 37-49.
33. He Z, Zou S, Yin J, Gao Z, Liu Y, Wu Y, et al. Inhibition of Endoplasmic Reticulum Stress Preserves the Integrity of Blood-Spinal Cord Barrier in Diabetic Rats Subjected to Spinal Cord Injury. Sci Rep. 2017; 7: 7661.
34. Koopmans GC, Deumens R, Honig WM, Hamers FP, Steinbusch HW, Joosten EA. The assessment of locomotor function in spinal cord injured rats: the importance of objective analysis of coordination. Journal of neurotrauma. 2005; 22: 214-25.
35. Zhu S-P, Wang Z-G, Zhao Y-Z, Wu J, Shi H-X, Ye L-B, et al. Gelatin nanostructured lipid carriers incorporating nerve growth factor inhibit endoplasmic reticulum stress-induced apoptosis and improve recovery in spinal cord injury. Molecular neurobiology. 2016; 53: 4375-86.
36. Hellal F, Hurtado A, Ruschel J, Flynn KC, Laskowski CJ, Umlauf M, et al. Microtubule stabilization reduces scarring and causes axon regeneration after spinal cord injury. Science. 2011; 331: 928-31.
37. Perale G, Rossi F, Santoro M, Peviani M, Papa S, Llupi D, et al. Multiple drug delivery hydrogel system for spinal cord injury repair strategies. J Control Release. 2012; 159: 271-80.
38. Zhang B, Gensel JC. Is neuroinflammation in the injured spinal cord different than in the brain? Examining intrinsic differences between the brain and spinal cord. Exp Neurol. 2014; 258: 112-20.
39. Zajac E, Schweighofer B, Kupriyanova TA, Juncker-Jensen A, Minder P, Quigley JP, et al. Angiogenic capacity of M1- and M2-polarized macrophages is determined by the levels of TIMP-1 complexed with their secreted proMMP-9. Blood. 2013; 122: 4054-67.
40. Adams KL, Gallo V. The diversity and disparity of the glial scar. Nat Neurosci. 2018; 21: 9-15.
41. Anderson MA, Burda JE, Ren Y, Ao Y, O'Shea TM, Kawaguchi R, et al. Astrocyte scar formation aids central nervous system axon regeneration. Nature. 2016; 532: 195.
42. Ruschel J, Bradke F. Systemic administration of epothilone D improves functional recovery of walking after rat spinal cord contusion injury. Exp Neurol. 2018; 306: 243-9.
43. Gaudet AD, Popovich PG. Extracellular matrix regulation of inflammation in the healthy and injured spinal cord. Exp Neurol. 2014; 258: 24-34.
44. Condic M, Letourneau P. Ligand-induced changes in integrin expression regulate neuronal adhesion and neurite outgrowth. Nature. 1997; 389: 852.
45. Fuhrmann T, Anandakumaran PN, Shoichet MS. Combinatorial Therapies After Spinal Cord Injury: How Can Biomaterials Help? Adv Healthc Mater. 2017; 6: 201601130.
46. Raspa A, Pugliese R, Maleki M, Gelain F. Recent therapeutic approaches for spinal cord injury. Biotechnol Bioeng. 2016; 113: 253-9.
47. Kahn OI, Baas PW. Microtubules and Growth Cones: Motors Drive the Turn. Trends Neurosci. 2016; 39: 433-40.
48. Wu QF, Yang L, Li S, Wang Q, Yuan XB, Gao X, et al. Fibroblast growth factor 13 is a microtubule-stabilizing protein regulating neuronal polarization and migration. Cell. 2012; 149: 1549-64.
49. Tam RY, Fuehrmann T, Mitrousis N, Shoichet MS. Regenerative therapies for central nervous system diseases: a biomaterials approach. Neuropsychopharmacology. 2014; 39: 169-88.
50. Zhang Y, Gu Z, Qiu G, Song Y. Combination of chondroitinase ABC, glial cell line-derived neurotrophic factor and Nogo A antibody delayed-release microspheres promotes the functional recovery of spinal cord injury. J Craniofac Surg. 2013; 24: 2153-7.
51. Wilems TS, Pardieck J, Iyer N, Sakiyama-Elbert SE. Combination therapy of stem cell derived neural progenitors and drug delivery of anti-inhibitory molecules for spinal cord injury. Acta biomaterialia. 2015; 28: 23-32.
52. Xiao Z, Tang F, Tang J, Yang H, Zhao Y, Chen B, et al. One-year clinical study of NeuroRegen scaffold implantation following scar resection in complete chronic spinal cord injury patients. Sci China Life Sci. 2016; 59: 647-55.

53. Siebert JR, Eade AM, Osterhout DJ. Biomaterial Approaches to Enhancing Neurorestoration after Spinal Cord Injury: Strategies for Overcoming Inherent Biological Obstacles. Biomed Res Int. 2015; 2015: 752572.
54. Lu C, Meng D, Cao J, Xiao Z, Cui Y, Fan J, et al. Collagen scaffolds combined with collagen-binding ciliary neurotrophic factor facilitate facial nerve repair in mini-pigs. Journal of Biomedical Materials Research Part A. 2015; 103: 1669-76.
55. Burnside ER, Bradbury EJ. Manipulating the extracellular matrix and its role in brain and spinal cord plasticity and repair. Neuropathol Appl Neurobiol. 2014; 40: 26-59.
56. Witte H, Neukirchen D, Bradke F. Microtubule stabilization specifies initial neuronal polarization. J Cell Biol. 2008; 180: 619-32.
57. Roman JA, Reucroft I, Martin RA, Hurtado A, Mao HQ. Local Release of Paclitaxel from Aligned, Electrospun Microfibers Promotes Axonal Extension. Adv Healthc Mater. 2016; 5: 2628-35.
58. Nagai J, Takaya R, Piao W, Goshima Y, Ohshima T. Deletion of Crmp4 attenuates CSPG-induced inhibition of axonal growth and induces nociceptive recovery after spinal cord injury. Mol Cell Neurosci. 2016; 74: 42-8.
59. Hackett AR, Lee JK. Understanding the NG2 Glial Scar after Spinal Cord Injury. Front Neurol. 2016; 7: 199.
60. Gordon-Weeks PR. Microtubules and growth cone function. J Neurobiol. 2004; 58: 70-83.
61. He Z, Jin Y. Intrinsic Control of Axon Regeneration. Neuron. 2016; 90: 437-51.
62. Li H, Wu W. Microtubule stabilization promoted axonal regeneration and functional recovery after spinal root avulsion. Eur J Neurosci. 2017; 46: 1650-62.
63. Neukirchen D, Bradke F. Cytoplasmic linker proteins regulate neuronal polarization through microtubule and growth cone dynamics. J Neurosci. 2011; 31: 1528-38.
64. Yamout A, Spec A, Cosmano J, Kashyap M, Rochlin MW. Neurotrophic factor receptor expression and in vitro nerve growth of geniculate ganglion neurons that supply divergent nerves. Dev Neurosci. 2005; 27: 288-98.
65. Gryz EA, Meakin SO. Acidic substitution of the activation loop tyrosines in TrkA supports nerve growth factor-dependent, but not nerve growth factor-independent, differentiation and cell cycle arrest in the human neuroblastoma cell line, SY5Y. Oncogene. 2003; 22: 8774-85.
66. Michael GJ, Averill S, Nitkunan A, Rattray M, Bennett DL, Yan Q, et al. Nerve growth factor treatment increases brain-derived neurotrophic factor selectively in TrkA-expressing dorsal root ganglion cells and in their central terminations within the spinal cord. J Neurosci. 1997; 17: 8476-90.
67. Zhou B, Yu P, Lin M-Y, Sun T, Chen Y, Sheng Z-H. Facilitation of axon regeneration by enhancing mitochondrial transport and rescuing energy deficits. J Cell Biol. 2016; 214: 103-19.
68. Luo X, Ribeiro M, Bray ER, Lee D-H, Yungher BJ, Mehta ST, et al. Enhanced transcriptional activity and mitochondrial localization of STAT3 co-induce axon regrowth in the adult central nervous system. Cell reports. 2016; 15: 398-410.
69. Deng C, Li M, Qian J, Hu Q, Huang M, Lin Q, et al. A Study of Different Doped Metal Cations on the Physicochemical Properties and Catalytic Activities of Ce20 M1 Ox (M=Zr, Cr, Mn, Fe, Co, Sn) Composite Oxides for Nitric Oxide Reduction by Carbon Monoxide. Chem Asian J. 2016; 11: 2144-56.
70. Moyano P, de Frias M, Lobo M, Anadon MJ, Sola E, Pelayo A, et al. Cadmium induced ROS alters M1 and M3 receptors, leading to SN56 cholinergic neuronal loss, through AChE variants disruption. Toxicology. 2018; 394: 54-62.
71. Gaudet AD, Popovich PG. Extracellular matrix regulation of inflammation in the healthy and injured spinal cord. Experimental neurology. 2014; 258: 24-34.
72. Haque A, Polcyn R, Matzelle D, Banik NL. New Insights into the Role of Neuron-Specific Enolase in Neuro-Inflammation, Neurodegeneration, and Neuroprotection. Brain sciences. 2018; 8: 33.